EPJ Web of Conferences **292**, 08002 (2024) https://doi.org/10.1051/epjconf/202429208002
NRM2023

Energy-dependent fission-product yields in the region of second-chance fission

Anton P. Tonchev[1,3*] *Ronald* C. Malone[1], *Anthony* P.D. Ramirez[1], *Jack* A. Silano[1], *Mark* A. Stoyer[1], *Mathew* E. Gooden[2], *Todd* A. Bredeweg[2], *David* J. Vieira[2], *Jerry* B. Wilhelmy[2], *Sean* W. Finch[3,4], *Calvin* R. Howell[3,4], and *Werner* Tornow[3,4]

[1]Lawrence Livermore National Laboratory, Livermore, California, USA
[2]Los Alamos National Laboratory, Los Alamos, New Mexico, USA
[3]Duke University, Durham, North Carolina, USA
[4]Triangle Universities Nuclear Laboratory, Durham, North Carolina, USA

Abstract. The energy dependence of high-yield fission products has been measured using quasi-monoenergetic neutron beams at energies between 5.5 and 11.0 MeV. The absolute number of fissions during the irradiation period was determined via dual-fission ionization chambers, while the fission products were measured via direct γ-ray spectroscopy. This paper presents absolute fission product yields from neutron-induced fission of ^{235}U, ^{238}U, and ^{239}Pu isotopes for five incident energies in the second chance fission region.

1 Introduction

The distribution of fragment masses following fission is one of the most basic quantities that has been observed since the discovery of fission by Hahn and Strassmann in 1938 [1,2]. The fission yields play an important role in many applications, such as development of advanced reactor and transmutation systems, estimation of decay heat and delayed neutron emission in nuclear reactors, studies of the reactor anti-neutrino anomaly, fission in the galactic chemical evolution, national security, and so on. In large part, for these reasons, the demand for high-quality fission product yield (FPY) data in such applications is rapidly increasing. Unfortunately, the current evaluated FPY data files contain only three energy points: thermal, fast, and 14-MeV incident neutron energies.

Evaluations of available FPY data by Chadwick *et al.* [3] and Thompson *et al.* [4] presented compelling evidence for a positive energy dependence for some high-yield fission products from neutron-induced fission of ^{239}Pu in the low-energy region between 0.2 and 2 MeV incident neutron energy. However, the data producing this energy dependence were made on critical assemblies and fast reactors, which have rather broad energy distributions. The lack of completeness and systematic studies of these cumulative FPYs in a broad energy range was the main motivation for the LLNL-LANL-TUNL collaboration. In this paper, the FPYs from neutron-induced fission of ^{235}U, ^{238}U, and ^{239}Pu at E_n = 5.5, 6.5, 7.5, 9.0, and 11.0 MeV, covering the region of the second chance fission, will be presented.

* e-mail: tonchev2@llnl.gov

2 Experimental details and analysis

These experiments have been performed at Triangle Universities Nuclear Laboratory (TUNL) using a 10 MV FN tandem Van de Graaff accelerator. High yields of fast quasi-monoenergetic neutrons of 5.5, 6.5, 7.5, 9.0, and 11.0 MeV were produced via the ^{2}H(d,n)^{3}He reaction. A schematic of our experimental setup is shown in Fig. 1. A dual-fission chamber (DFC) was positioned in close proximity (4 cm) to the neutron production source. The average neutron flux at the center of the FC was measured to be from $6x10^{7}$-$2x10^{8}$ n·s^{-1}·cm^{-2} for energies from 6.5 to 11.0 MeV, respectively. Significant effort was spent performing different TOF and activation measurements to characterize the neutron beam conditions at the TUNL TOF room with respect to the produced neutron fluxes, their energy spreads, and the contribution of neutrons scattered from the target room walls [6].

The DFCs contain two thin (~100 μg/cm^{2}) reference foils and a thicker (~200 mg/cm^{2}) actinide activation target [5]. The activation target is contained in the center of the chamber while the thin reference foils are up- and down-stream from the activation target. The thick activation target is composed of the same actinide material as the thin reference foils in the adjacent chambers. The advantage of using the DFC method, compared to other methods such as radiochemistry, the ratio method, or mass separation, is that the total number of fissions in the target can be determined without having to explicitly know either the neutron-induced fission cross section or the neutron flux, thus greatly reducing the total uncertainty of the measurements. Only the ratio of the masses of the thin reference foils to the thick activation target must be known.

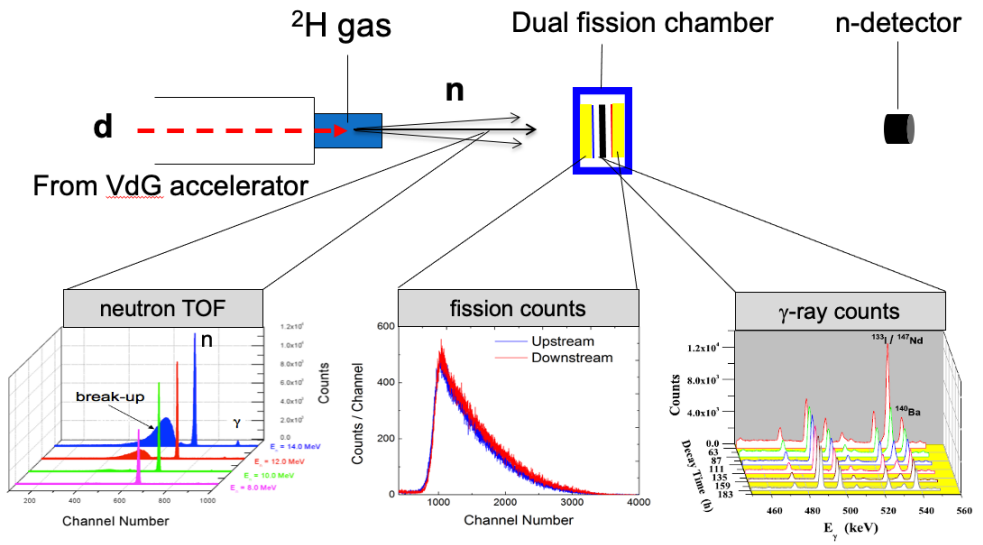

Fig. 1. Schematic of the FPY experimental setup at TUNL. The bottom left panel shows the measured TOF neutron spectra, the bottom middle panel shows the DFC pulse-height spectrum measured during the irradiation time, and the bottom right panel shows the time evolution of the γ-ray spectra measured for different time intervals after the end of irradiation.

Following neutron activation, we removed the thick target from the DFC and continuously counted the emitted γ rays using large-volume high-purity germanium (HPGe) detectors. The γ-ray counting started about 20 minutes after the end of irradiation and

continued for a period of 2-3 months. We followed the decay time of each fission product in order to uniquely identify the fission product and ensure the particular γ-ray line was free of interference. This also allowed us to optimize the counting time for each γ-ray peak based on half-life and the signal-to-background ratio, providing the lowest possible detection limit and minimizing the uncertainties in the determined FPYs.

The total fission rate in the thick activation target is calculated from each chamber according to:

$$F_{Ti} = \frac{N_{fi}}{\varepsilon_{FCi}\, t_{LT}} \frac{m_{thick}\, R_{thick}}{m_{thin,i} R_{thin,i}} C_{Boost} C_{Flux} \quad (1)$$

where i designates the fission chamber under consideration (DFC_1 (downstream) or DFC_2 (upstream)), N_{fi} is the total number of fission counts in chamber i during the irradiation time, $m_{thick(thin,i)}$ is the mass of the thick (thin) foil, $R_{thick(thin,i)}$ is the mass fraction of the actinide of interest in the thick (thin) foil, ϵ_{FCi} is the efficiency of the fission chamber, t_{LT} is the live time of the data-acquisition system during irradiation time, $C_{Boost,i}$ is the kinematic boosting correction for the upstream and downstream DFCs, and $C_{Flux,i}$ is the correction factor to convert the neutron flux at the position of reference foil i to the neutron flux at the position of the activation foil.

The fission rate in the thick target is determined by taking a weighted average for F_{T1} and F_{T2}:

$$F_T = \frac{w_1 F_{T1} + w_2 F_{T2}}{w_1 + w_2}, \qquad w_i = \frac{1}{\sigma_i^2}, \quad (2)$$

where σ_i is the uncertainty in the fission chamber counts including statistical uncertainty, the chamber efficiency, the kinematic boost correction C_{Boost}, and the flux correction C_{Flux}.

After irradiation, the induced FPY activity in the activation foil is measured by two designated HPGe detectors. The individual FPY is calculated by using the following activation equation:

$$FPY_i = \frac{\lambda_i S_i}{F_T I_\gamma \epsilon_\gamma(E_i) f_i(t)} C_{Att} C_{Sum} C_{Beam} C_{Iso} C_{Break} \quad (3)$$

where λ_i is the decay constant, S_i is the number of observed γ rays in the photo-peak area, F_T is the corrected fission rate in reference target determined from Eqs. (1) and (2), I_γ is the γ-ray intensity (also called branching ratio), $\epsilon_\gamma(E_i)$ is the HPGe detector efficiency at the energy of the emitted γ ray, $f_i(t)$ is the time correction factor accounting for the irradiation t_{irr}, decay t_d, and measurement times t_m and is given as: $f_i(t) = \left(1 - e^{-\lambda_i t_{irr}}\right)\left(e^{-\lambda_i t_d}\right)\left(1 - e^{-\lambda_i t_m}\right)$, C_{Att} is the point-to-volume source correction factor including γ-ray self-attenuation, C_{Sum} is the coincidence summing correction, C_{Beam} is the beam fluctuation correction, C_{Iso} is the correction for isotopic impurities in the targets, and C_{Break} is the off-energy neutron correction. More detailed descriptions of these correction factors are given in the Refs. [7-9].

3 Results and Discussion

The experimental results from the six most relevant cumulative FPYs of ^{147}Nd, ^{143}Ce, ^{140}Ba, ^{99}Mo, ^{97}Zr, and ^{95}Zr from neutron-induced fission of ^{239}Pu, ^{235}U, and ^{238}U at 5.5, 6.5, 7.5, 9.0, and 11.0 MeV are shown in Figs. 2 and 3. These are the mid-energy FPYs which fill the gap between our previously published data from E_n = 0.58, 1.37, 2.37, 3.6, 4.49, 5.5, 8.9, and 14.8 MeV [6]. The error bars represent the total uncertainties. Note that ^{95}Zr, ^{97}Zr, and ^{99}Mo fission products are at the peak of the left mass asymmetric peak distribution, while ^{140}Ba, ^{143}Ce, and

^{147}Nd are situated at the right mass asymmetric peak distribution. Data analysis was significantly improved relative to previous work [6], providing a more quantitative basis for evaluating these cumulative FPY data for basic and applied physics. As has been described, many correction factors have been improved, such as FC efficiency and kinematic boosting, Monte-Carlo neutron source and FC chamber geometry, detector efficiency, cascade summing, and others – increasing the fidelity of the current measurements [7-9]. Additionally, the uncertainties associated with the parameters in Eqs. (1) and (3) were carefully quantified and updated to better reflect the precision of our measurements.

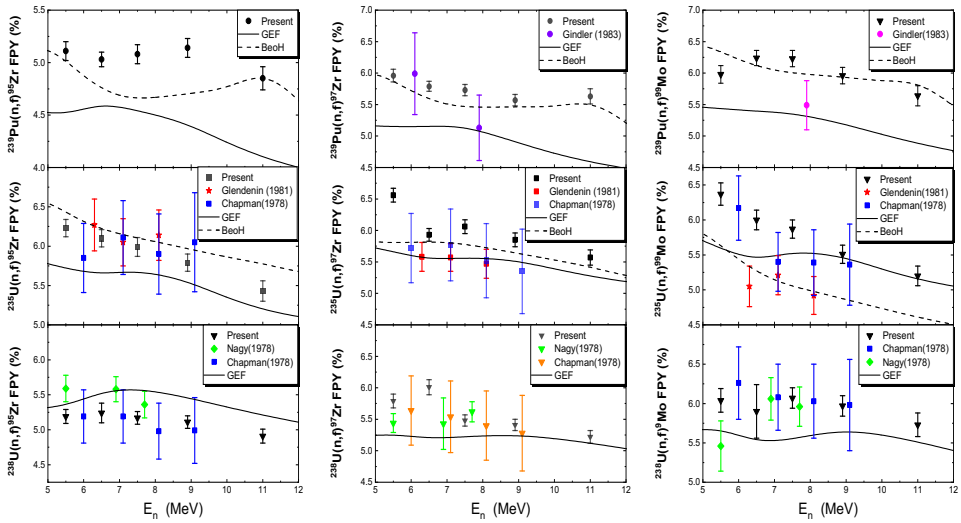

Fig. 2. Fission product yields of ^{95}Zr (left), ^{97}Zr (center), and ^{99}Mo (right) as a function of monoenergetic neutrons for fission of ^{239}Pu (top row), ^{235}U (middle row), and ^{238}U (bottom row) in comparison to the available literature data [10-13] and GEF and BeoH calculations [14-16]. Both present and literature data are presented with their total uncertainty.

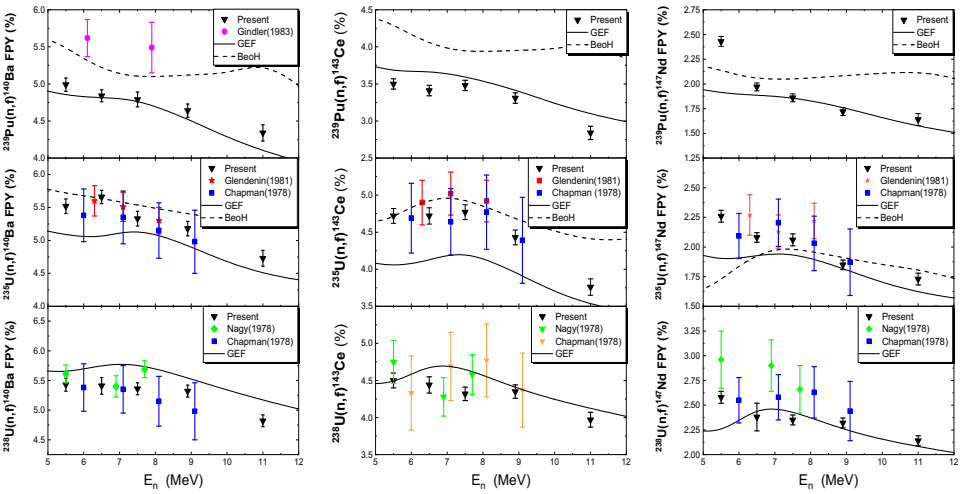

Fig. 3. Fission product yields of ^{140}Ba (left), ^{143}Ce (center), and ^{147}Nd (right) as a function of monoenergetic neutrons for fission of ^{239}Pu (top row), ^{235}U (middle row), and ^{238}U (bottomrow) in

comparison to the available literature data [10-13] and GEF and BeoH calculations [14-16]. Both present and literature data are presented with their total uncertainty.

The available literature data [10-13] of the cumulative FPYs for the three actinide targets in the energy region of the second chance fission are also shown in Figs. 2 and 3. While there is an overall agreement between the literature data and our current FPY results, significant improvement of the recent one makes the declining trend of these high-yield FPYs more convincing.

Furthermore, the decrease of FPYs in the second chance fission region is depicted by the semiempirical GEneral description of Fission observables (GEF 2023/2.2) model [14]. All the GEF results have been obtained with the same default parameter set – no local parameter adjustment has been made. Our current results are also in very good agreement with the yields predicted by the BeoH multi-chance fission model as well [15]. The BeoH calculations are presented only for ^{239}Pu and ^{235}U neutron-induced fission [15,16]. Both codes calculate a wide range of pre- and post-neutron fission observables in neutron-induced fission. The multi-chance fission (fission after neutron emission) is also implemented in GEF and BeoH codes. The GEF calculations show a very good agreement for ^{147}Nd cumulative FPY for all fissioning systems and underestimation of the ^{95}Zr, ^{97}Zr, and ^{99}Mo FPYs for ^{239}Pu(n,f). In contrast, the BeoH model provides a very good prediction for the fission products that are at the peak of the left mass asymmetric peak distribution but overpredicts the FPYs of the right mass asymmetric peak distribution for ^{239}Pu(n,f). The new mid-energy data show a steady decrease of the major FPYs as a function of neutron energy. Combined with our previous data [6] this trend is consistent with FPYs toward 14.8 MeV energy. The negative slope is due to increasing of the so-called symmetric fission mode which increases with increasing incident energy. There is no visible change or kink in the slope of these FPYs which might be affected by the opening of the third-chance fission channel around E_n=11.0 MeV.

In Fig. 4 we compared the fission yields of the same selected products at five incident neutron energies as a function of ^{235}U and ^{238}U targets. The data points are presented with their absolute uncertainty.

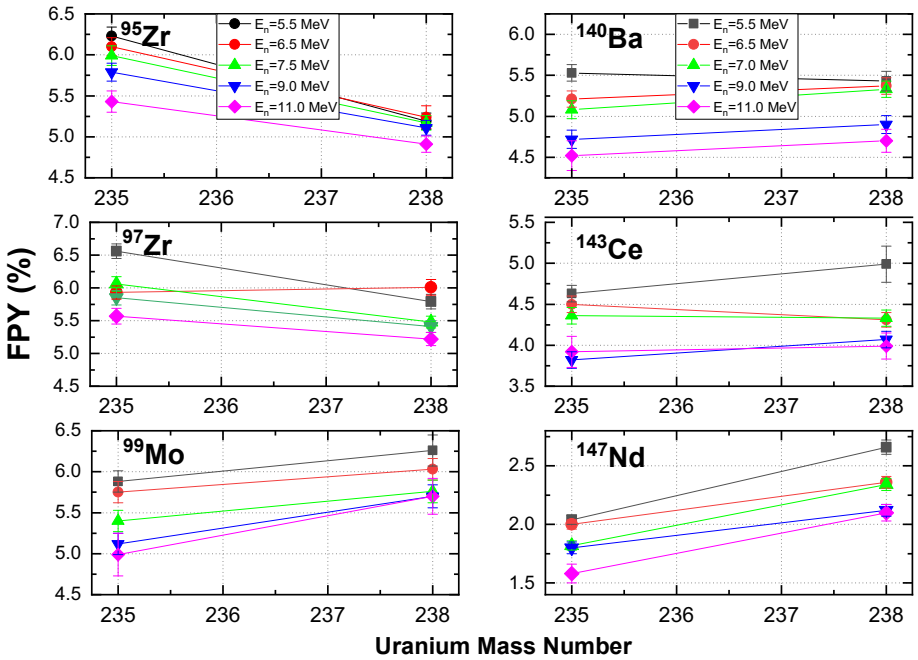

Fig. 4. Cumulative FPYs of ^{95}Zr, ^{97}Zr, ^{99}Mo, ^{140}Ba, ^{143}Ce, and ^{147}Nd from neutron-induced fission of ^{235}U and ^{238}U at six incident neutron energies.

As can be seen, the yields of various products exhibit different trends when the uranium mass number changes from *A=235* to *A=238*. This picture is consistent for almost all incident neutron energies in the region between the second and third-chance fission. For example, the FPYs of ^{95}Zr and ^{97}Zr decrease with increasing the mass number of the fissile isotope, while the FPYs for the remaining isotopes increase with increasing of the fissile number.

Our selected FPYs from neutron-induced fission on ^{235}U and ^{238}U isotopes can be compared with the same fission yields from other available uranium targets, such as *A=233, 234*, and *236* [17,18]. In these references, the authors debated whether particular FPYs vary smoothly with uranium mass number. In Fig. 5, the same six FPYs from Fig. 4 are compared with the literature data from the fission of ^{233}U, ^{234}U, ^{235}U, ^{236}U, and ^{238}U, where the mass trend can be followed only with 14.8 MeV neutrons. Our cumulative FPY data is in a good agreement with the available literature data and confirms the conclusion from Ref. [18] that the fission yields of these high-yield products vary smoothly with uranium target mass number. It will be interesting to follow this dependence for neutron energies in the region of the second-chance fission.

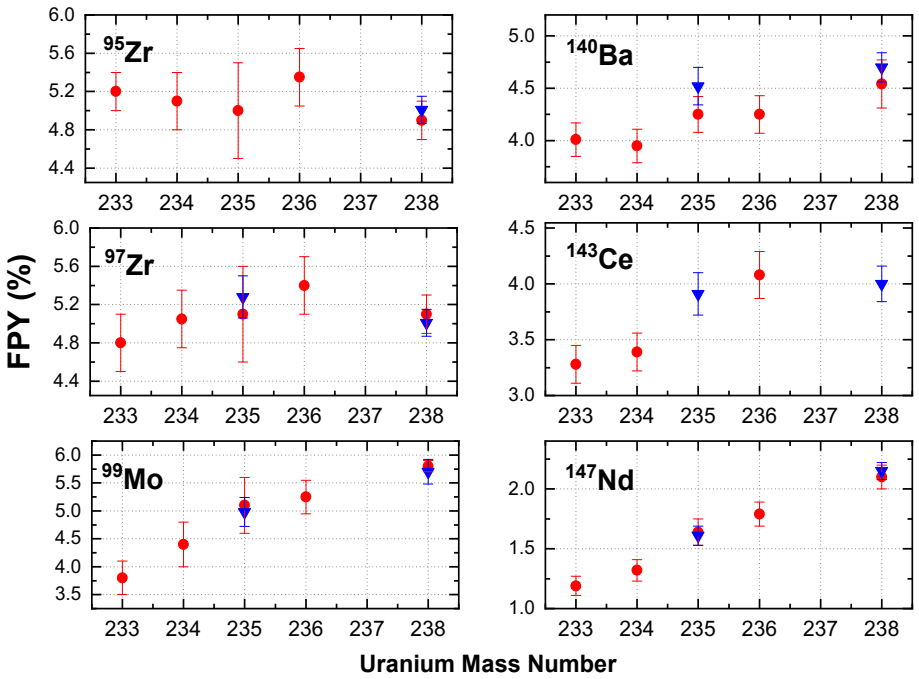

Fig. 5. Cumulative FPYs of ^{95}Zr, ^{97}Zr, ^{99}Mo, ^{140}Ba, ^{143}Ce, and ^{147}Nd at E_n=14.8 MeV as a function of uranium mass number. Current FPY data from ^{235,238}U(n,f) is shown with upside-down triangles, while the literature data from Ref. [17, 18] is shown with circles.

4 Summary

The new FPY data in the mid-energy or second-chance fission region show a steady decrease as a function of incident neutron energy for all three actinides. This trend is consistent with the fission models implemented in GEF [14] and BeoH [15] codes. Considering FPYs near the valley of the mass distribution, described by the so-called super-long mode, we observe a steady increase in the measured fission yield with neutron energy. There is no visible change in the slope of these FPYs which might be affected by third-chance fission opening up around 11 MeV. It should be noted that our new FPY data are largely consistent with the existing literature data [10-13,17,18]. The data analysis was significantly improved providing more substantial basis for the evaluation of these cumulative FPY data.

Acknowledgments

This work was supported by the US Department of Energy through Lawrence Livermore National Laboratory under contract DE-AC52-07NA27344 and the Los Alamos National Laboratory under contract No. 89233218CNA000001. This work was also supported in part by the National Nuclear Security Administration Stewardship Science Academic Alliances grant no. DE-NA0002936, and the U.S. Department of Energy, Office of Nuclear Physics, under grant no. DE-FG02-97ER41033.

References

1. O. Hahn and F. Strassmann, Naturwissenschaften **27**, 11 (1939)
2. L. Meitner and O. R. Frisch, Nature **143**, 239 (1939)
3. M. B. Chadwick et al., Nuclear Data Sheets **111**, 2923 (2010)
4. I. J. Thompson, Y. M. X. M. Dardenne, J. M. Kenneally, A. Robertson, L. E. Ahle, C. A. Hagmann, R. A. Henderson, D. Vogt, C.-Y. Wu, and W. Younes, Nuclear Science and Engineering **171**, 85 (2012)
5. C. Bhatia, B. Fallin, M.E. Gooden, C.R. Howell, J.H. Kelley, W. Tornow, C.W. Arnold, E.M. Bond, T.A. Bredeweg, M.M. Fowler, W.A. Moody, R.S. Rundberg, G. Rusev, D.J. Vieira, J.B. Wilhelmy, J.A. Becker, R. Macri, C. Ryan, S.A. Sheets, M.A. Stoyer, A.P. Tonchev, Nucl. Instrum. Methods Phys. Res. A **757**, 7 (2014)
6. M. E. Gooden, B. Fallin, C. R. Howell, J. H. Kelley, W. Tornow, C. W. Arnold, E. M. Bond, T. A. Bredeweg, M. M. Fowler, W. A. Moody, R. S. Rundberg, G. Rusev, D. J. Vieira, J. B. Wilhelmy, J. A. Becker, R. Macri, C. Ryan, S. A. Sheets, M. A. Stoyer, and A. P. Tonchev. Nuclear Data Sheets 131, 319 (2016)
7. A. Tonchev, J. Silano, A. Ramirez, R. Malone, LLNL-TR-839369 (2022)
8. A. P. D. Ramirez, J. A. Silano, R. C. Malone, M. A. Stoyer, A. P. Tonchev, M. E. Gooden, J. B. Wilhelmy, S. W. Finch, C. R. Howell, Krishichayan, and W. Tornow Phys. Rev. C **107**, 054608 (2023)
9. M. Gooden, A.P.D. Ramirez, T.A. Bredeweg, E.M. Bond, S.W. Finch, C.R. Howell, Krishichayan, R.C. Malone, J.A. Silano, M.A. Stoyer, A.P. Tonchev, W. Tornow, D. Vieira, and J.B. Wilhelmy (submitted to Phys. Rev. C)
10. T. C. Chapman, G. A. Anzelon, G. C. Spitale, and D. R. Nethaway, Phys. Rev. C **17**, 1089 (1978)
11. S. Nagy, K. F. Flynn, J. E. Gindler, J. W. Meadows, and L. E. Glendenin, Phys. Rev. C **17**, 163 (1978)
12. L. E. Glendenin, J. E. Gindler, D. J. Henderson, and J. W. Meadows, Phys. Rev. C **24**, 2600 (1981)
13. J. E. Gindler, L. E. Glendenin, D. J. Henderson, and J. W. Meadows, Phys. Rev. C **27**, 2058 (1983)
14. K. H. Schmidt, B. Jurado, C. Amouroux, and C. Schmitt, Nuclear Data Sheets **131**, 107 (2016)
15. A. E. Lovell, T. Kawano, S. Okumura, M. R. Mumpower, I. Stetcu, and P. Talou. EPJ Web of Conferences **284**, 04015 (2023)
16. A. E. Lovell, T. Kawano, S. Okumura, I. Stetcu, M. R. Mumpower, and P. Talou. Phys. Rev. C 103, 014615 (2021)
17. D.R. Nethaway and B. Mendoza, Phys. Rev. C **5**, 1827 (1972)
18. D.R. Nethaway and B. Mendoza, Phys. Rev. C **6**, 1821 (1972)